A New Device for Two-Way Time-Frequency Real-Time Synchronization

Ke Zhang[1,2,3], Decai Zou[1,2,3], Pei Wang[1,3], Wenfang Jing[1,2,3]*

[1] National Time Service Center, Chinese Academy of Sciences, China
[2] University of Chinese Academy of Sciences, China
[3] Key Laboratory of Precision Navigation and Timing Technology, Chinese Academy of Sciences, China
zhangke@ntsc.ac.cn, zdc@ntsc.ac.cn, wangpei@ntsc.ac.cn, jingwf@ntsc.ac.cn

Abstract

The netted wireless sensor nodes or coherent accumulation processing in multistatic radar imaging requires high accuracy time synchronization. Although GNSS timing can also be used as a time synchronization method to serve the applications above, its timing accuracy will be limited. In this context, we present the hardware implementation for Two-Way Time-Frequency Real-Time Synchronization (TWTFRTS) with an automatic adaptive jitter elimination algorithm based on Kalman and PID, which is implemented in a real-time, low-cost, portable Xilinx ZYNQ device. A short (2 km) baseline TWTFRTS experiment was done with a pair of devices composed of a master device and a slave device. The result shows a high precision of time synchronization performance with the standard deviation (1 σ) better than 1 ns.

Keywords: Time-frequency synchronization, Microwave link, Kalman filter, PID control, ZYNQ

1 Introduction

The time synchronization requirements of multi-base radar imaging cover multiple synchronization scenarios such as ground-ground, ground-air, and air-air. The in-phase transmission and reception of signals between multi-base radars can help to perform high-resolution imaging of the target, whose requirement for time synchronization accuracy is challenging. For example, Ku-band multi-station imaging requires ns-level time synchronization accuracy, and coherent accumulation processing imaging requires 0.01ns-level time synchronization accuracy. The higher the frequency band and the shorter the wavelength, the higher the time synchronization accuracy requirements. In wireless sensor network nodes [1] and multistatic radar imaging, time synchronization methods based on Global Navigation Satellite System (GNSS) satellites are widely used. It mainly includes GNSS standard timing technology, GNSS Precise Point Positioning (PPP) timing technology [2], satellite timing technology based on Common View (CV) principle [3]. Their synchronization accuracy is usually within a few ns, and the accuracy is limited. Two-Way Satellite Time and Frequency Transfer (TWSTFT) [4-6] technology is a high-precision time transfer technology for international time comparison. In recent years, high-precision time-frequency transmission based on optical fiber has made great progress. However, signals based on optical fiber propagation are limited in optical fiber networks. The laying cost of optical fiber is high. In free space, high-precision time-frequency signals dissemination via microwave has shown great advantage of all-weather dissemination. At present, the accuracy of TWSTFT can reach 500~750ps, and the stability can reach 200 ps [7]. But usually TWSTFT is non-real-time, and the equipment used for TWSTFT is complicated and expensive. Affected by factors such as non-real-time working methods and heavy terminal equipment, it is not suitable for air-based scenarios. GPSDOs are widely used in measurement devices and communication systems due to their cost-effective, high-precision, and self-calibrating operation [8].This paper inherits the working principle of TWSTFT technology and combines GPS-Disciplined Oscillators (GPSDO) [9-12] technology to realize a low-cost, portable, real-time high-precision time-frequency synchronization device with an automatic adaptive jitter elimination algorithm based on Kalman and PID, which is implemented in a real-time, low-cost, portable Xilinx ZYNQ device. The result shows a high precision of time synchronization performance with the standard deviation (1 σ) better than 1 ns.

The remainder of this paper is organized as follows. The system model of the proposed FPGA-based TWTFRTS is presented in detail in Section 2, including the hardware implementation and software design of measurement and jitter elimination Algorithm. The experimental design and results are presented and discussed in Section 3. Finally, Section 4 summarizes the work in this paper.

2 Design of the System

This section mainly describes the implementation of TWTFRTS system, which is carried out from the hardware architecture and software algorithms.

2.1 Hardware Design

2.1.1 System Experimental Model

A single TWTFRTS device consists of baseband signal processing module, power amplifier and low noise amplifier, RF transceiver module, clock and frequency synthesis module, transceiver integrated antenna, chassis, power supply module, display and control module and other modules

*Corresponding Author: Decai Zou; E-mail: zdc@ntsc.ac.cn
DOI: 10.53106/160792642023052403024

composition. TWTFRTS devices are mounted on the space-based aircraft (slave) and the ground-based anchoring (master) station respectively, and form a two-way time comparison and time synchronization system through two-way ranging and two-way communication with each other. The device and system structure are shown in Figure 1. The Master and Slave work in pairs.

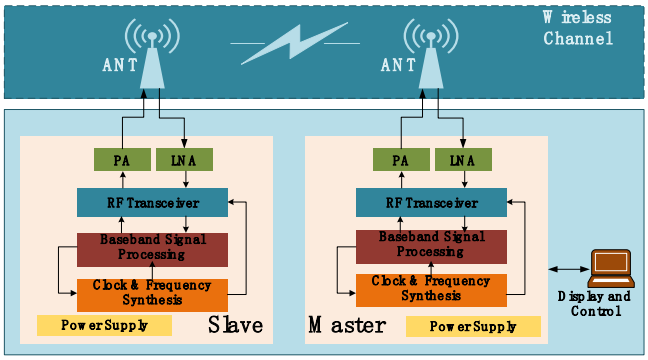

Figure 1. The structure of the TWTFRTS system

2.1.2 Structure of The Device

As shown in the Figure 2, the Master and the Slave are designed with the same hardware architecture.

SoC: The core chip of the baseband signal processing module is Xilinx ZYNQ 7045 SoC, which is equipped with dual-core ARM Cortex-A9 processors integrated with Kintex-7 based field-programmable gate array (FPGA). The Z-7045 is connected to peripherals such as RF transceiver module, clock and frequency synthesis module, FLASH memory, DDR3 memory, PC. Meanwhile, the debugging interface is also reserved.

PA & LNA: The power amplifier and the low noise amplifier are integrated in one module by analog circuit, which is connected with the integrated transceiver antenna and the RF transceiver module.

RF: The RF transceiver module is implemented by ADI AD9361, which includes uplink and downlink. After the uplink receives the digital signal from the FPGA, the digital signal is converted to the analog signal through the DAC. Then, the analog signal is up-converted to the radio frequency after filtering and amplifying, finally sent to the power amplifier. After the downlink receives the analog signal from the low-noise amplifier, the analog signal is converted into a digital signal by ADC, and then up-converted to the radio frequency after filtering and amplifying, and finally sent to the power amplifier.

Clock: The design of the clock and frequency synthesis module is one of the key elements for the TWTFRTS device to achieve high-precision time-frequency synchronization. The reference clock source input of this module includes two types of on-board voltage-controlled oven-controlled crystal oscillator (VC-OCXO) and external 10MHz clock, and can be switched through soft configuration. Typically, the master is in external 10MHz mode and the slave is in on-board VC-OXCO mode. The time difference calculated by the A9 drives a digital-to-analogue converter (DAC) which steers the 10MHz oscillator to compensate accurately for the measured phase discrepancy. After phase locking and clock distribution, the 10MHz clock reference signal provides the same source time-frequency signal to the RF transceiver module and the baseband signal processing module (FPGA), and provides the 100MHz frequency signal to external users. The differential 1PPS signal time output by the FPGA based on the homologous reference first passes through the differential-to-single-ended circuit, and then passes through the clock buffer and then sends it to the external user.

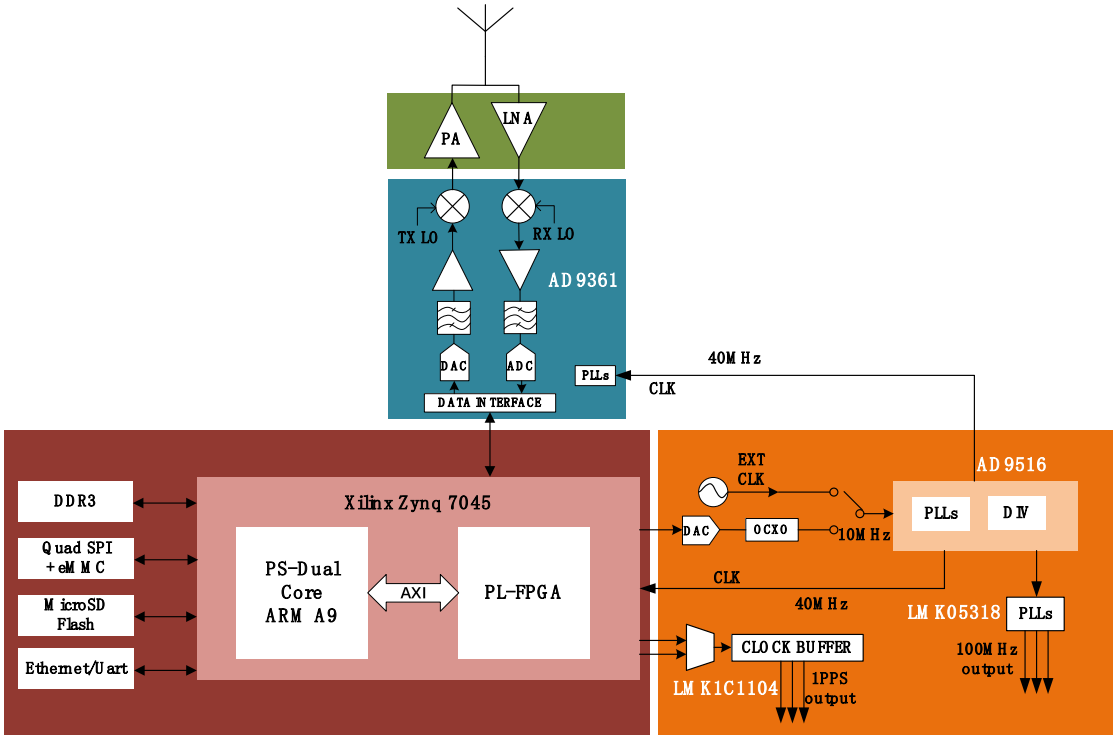

Figure 2. The structure of the TWTFRTS device

2.2 Software Design

2.2.1 Basic Principles of Two-Way Time-Frequency Real-Time Synchronization

The principle of the two-way time comparison technique adopted in this paper is inherited from the principle of Two-Way Satellite Time and Frequency Transfer (TWSTFT) [4]. Different from TWSTFT, the two-way time comparison technology in this paper is that two devices send and receive directly in pairs, without satellite forwarding.

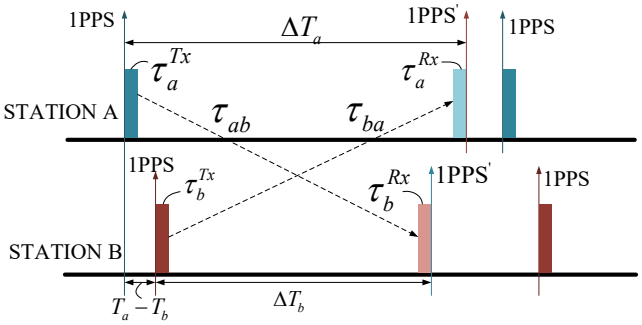

Figure 3. Two-way time synchronization working principle diagram

As shown in Figure 3, the ground Master station A and the load Slave station B, the two stations work in pairs. The unknowns between the two stations that need to be measured are: the time difference between the two stations and the distance between the two stations. We need each station to transmit a signal and measure the phase of its own transmitted signal and the phase of the received signal from the other station. In engineering practice, the baseband module transmitting unit will modulate a time signal (for example, a single pulse second signal (1PPS, 1 pulse per second)) into a pseudo-random noise code (PRN), and then transmit it through the radio frequency unit, via the wireless link reach the receiving end. The receiving unit will demodulate this second signal and reproduce the received 1PPS from the originator. The time interval measurement is performed at the two sites at the same time. The 1 PPS signals generated by the local clocks of the two sites respectively start the local time interval counter. After receiving the 1PPS signal from the opposite end, the time interval count ends once, and the time difference between the two 1PPS signals is obtained. That is, the time difference observations are obtained based on the two stations. Based on the symmetry of the microwave bidirectional path, the clock difference of the reference clocks of the two stations can be obtained by exchanging the time difference measurement value obtained by the two stations, and then calculating the difference value. The time difference between the local clocks of two sites can be described as:

$$T_a - T_b = (\Delta T_a - \Delta T_b)/2 + [(\tau_a^{Tx} + \tau_b^{Rx}) - (\tau_b^{Tx} + \tau_a^{Rx})]/2 + (\tau_{ab} - \tau_{ba})/2. \quad (1)$$

where the first term on the right side of the equation is the difference between the measured values of the two stations A and B. The local time interval count observations of the two stations are debugged into the wireless signals between the two stations in the form of communication data. The measurement value of the opposite site can be obtained through the wireless communication link.

The second term on the right side of the equation, which includes the equipment delays of the two links, is the difference between the equipment delays in the two propagation directions.

The third term on the right side of the equation is the propagation path delay, which can be ignored for an ideally symmetric link.

The derivation process of the above formula (1):

$$\Delta T_a = (T_a - T_b) + \tau_b^{Tx} + \tau_{ba} + \tau_a^{Rx}. \quad (2)$$

$$\Delta T_b = \tau_a^{Tx} + \tau_{ab} + \tau_b^{Rx} - (T_a - T_b). \quad (3)$$

(2) and (3) are the observation equations of station A and station B, respectively. The time difference can be obtained by subtracting the two formulas (2) and (3), and the distance measurement value can be obtained by adding the two formulas (2) and (3).

The baseband processing module of Slave B station performs preliminary adjustment of the local RTC (Real-Time Clock) according to the measured time difference value, obtains the initial frequency deviation between the two stations through the Doppler estimation of signal tracking, and at the same time, obtains the initial frequency deviation between the two stations through the measured time difference value and the local frequency synthesis The feedback loop of the output frequency reference dynamically adjusts the frequency and phase of the local clock in real time, and finally achieves convergence and synchronization with the master frequency reference and time reference. In actual engineering practice, it is necessary to establish different time difference measurement models for correction according to the relative magnitude relationship between the transmission delay between the master and slave stations and the clock difference between the two stations.

2.2.2 Software Arithmetic for Jitter Elimination Based on Kalman and PID

After the signal sent by the master station passes through the antenna and RF transceiver module of the slave station, it enters the baseband signal processing module of the slave station. The digital signal sampled and quantized by ADC is firstly captured and calculated in the FPGA. After the signal is successfully captured, the coarse code phase and carrier Doppler information are sent to the tracking control module, and then the digital signal is tracked. The time difference observation of the slave is extracted from the tracking loop of the slave, and sent to the ARM through the AXI bus between the FPGA and the ARM. At the same time, the time difference observation information transmitted by the master station is decoded and extracted in the ARM, and the difference calculation is made between the time difference observation value of the master station obtained by decoding and the time difference observation value extracted from the local tracking loop of the slave station. The jitter of the time difference value calculated ARM above is eliminated by Kalman filtering and PID control and then passed to the

DAC module. The DAC module adjusts the OCXO output according to the data transmitted by the ARM. Based on this, the reference clock signal of each module including the sampling clock is adjusted, so as to achieve the purpose of time synchronization. The software arithmetic is shown in Figure 4.

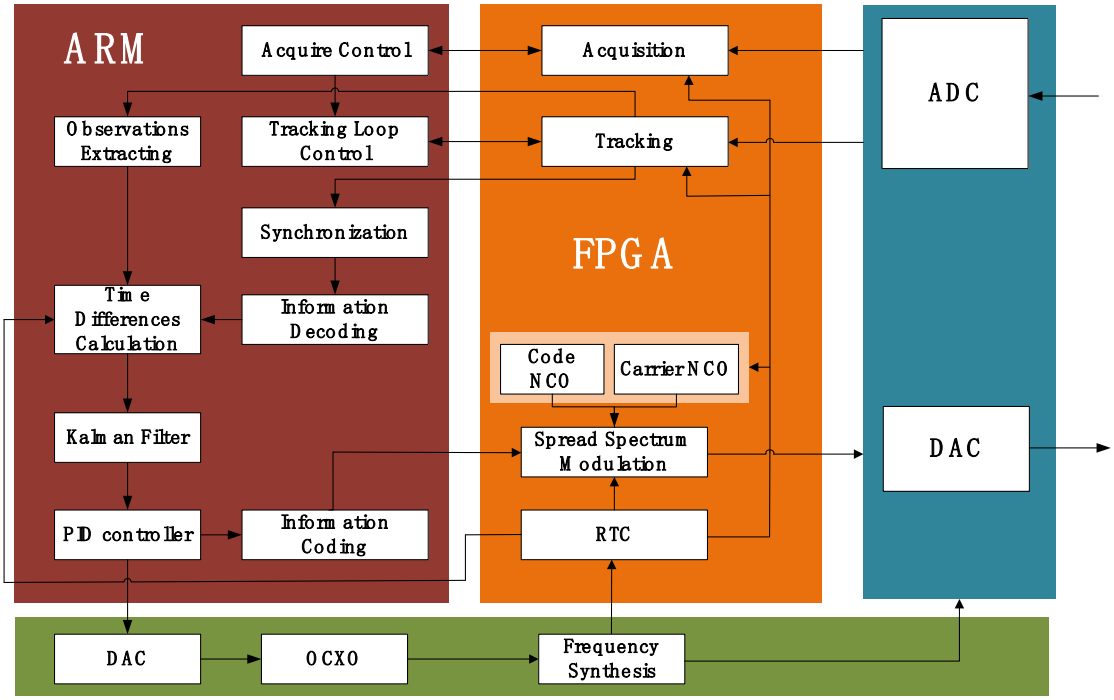

Figure 4. Software arithmetic

A. Kalman Filter

Kalman filtering is an iterative algorithm for solving optimal linear filtering and estimation problems based on the minimum mean square error criterion. Using Kalman filtering can reduce the influence of random phase jitter of the signal and measurement error on the system, and the processing has the characteristics of high real-time performance and small data storage.

The one-step prediction estimation result of the state of phase difference at time k is expressed as $\tilde{x}(k)$, the correction result of the measurement filter is expressed as $\hat{x}(k)$, and $z(k)$ is the observed quantity with interference, then the state prediction equation is as follows [11],

$$\tilde{x}(k) = a\hat{x}(k-1). \tag{4}$$

$$P_1(k) = a^2 P_e(k-1) + \delta_w^2. \tag{5}$$

The measurement update equation is as follows,

$$K(k) = cP_1(k) / (c^2 P_1(k) + \delta_v^2). \tag{6}$$

$$\hat{x}(k) = \tilde{x}(k) + K(k)[z(k) - c\tilde{x}(k)]. \tag{7}$$

$$P_e(k) = P_1(k) - cb(k)P_1(k). \tag{8}$$

where $K(k)$ is the time-varying gain, a and c are constant model coefficients (Applied in this paper, a = c = 1), δ_w^2, δ_v^2 are the model noise covariance. The initial state $\hat{x}(0)$ can be obtained by using the mean value of the $z(k)$ sequence collected at the beginning. According to the formula

$$P_e(0) = E[z(k) - \hat{x}(0)]^2. \tag{9}$$

the initialization value $P_e(0)$ can be obtained. The noise covariance δ_v^2 is generally set to 1.0, and δ_w^2 can be determined through experiments. The determined principle is to optimize the filtering effect. With these initial values and parameters, combined with each input data, the Kalman filter can iteratively run to obtain the filter estimated output at each moment.

B. PID Control

After the phase difference data is filtered by Kalman, the PID control algorithm is used to calculate the digital voltage control value corresponding to the frequency offset correction value. The digital voltage control value is converted into an analog signal by DAC to control the crystal oscillator.

Since this paper implements PID control through software in ARM processor, digital PID is required. PID is a linear controller that compares the input value $x(k)$ with the output value $y(k)$ to form the control deviation:

$$e(k) = x(k) - y(k). \tag{10}$$

After Proportional-Integral-Derivative operations are performed, the control quantity is formed by linear combination, as shown in the following Figure 5.

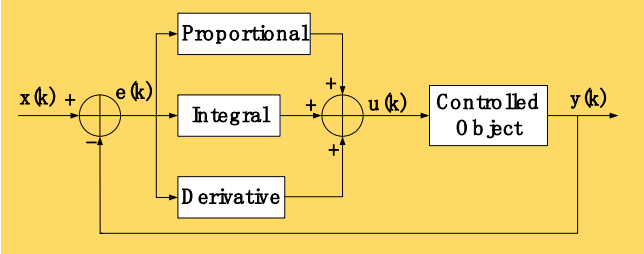

Figure 5. Block diagram of PID control theory

The discrete expression of PID control algorithm [11] is

$$u(k) = K_P[e(k) + \frac{1}{T_I} \cdot T\sum_{j=0}^{k} e(j) + T_D \cdot \frac{e(k) - e(k-1)}{T}]. \quad (11)$$

where K_P is the proportional coefficient, T_I is the integral time constant, T_D is the differential time constant, T is the sampling period, k is the sampling sequence number, $k = 0, 1, 2, \ldots$.

From the above formula (11), we can get,

$$\begin{aligned} u(k) &= u(k-1) + K_P\left\{[e(k) - e(k-1)] + \frac{T}{T_I} \times e(k) + \frac{T_D}{T}[e(k) - 2e(k-1) + e(k-2)]\right\} \\ &= u(k-1) + K_P\left(1 + \frac{T}{T_I} + \frac{T_D}{T}\right) \times e(k) - K_P\left(1 + \frac{2T_D}{T}\right) \times e(k-1) + K_P \frac{T_D}{T} \times e(k-2). \end{aligned} \quad (12)$$

In engineering applications, on the one hand, in order to deal with the saturation effect of PID control, the accumulation of the integral term should not be too large. When $u(k)$ exceeds a certain set interval, the difference term $e(k)$ will not be included in the integral accumulation. On the other hand, to avoid the large oscillation of the system caused by the excessive control value, we set a threshold for the difference term $e(k)$. Integral accumulation is performed only when the difference term $e(k)$ is within the threshold.

3 Experiments and Discussions

In order to verify the time-frequency synchronization performance of the device implemented in this paper, a 2km wireless flight test scenario is designed to verify the time synchronization performance (as shown in Figure 8), and a static wireless scenario is designed to verify the frequency synchronization performance (as shown in Figure 6).

3.1 Time Synchronization

In order to verify the time synchronization performance between the Master device and the Slave device, as shown in Figure 8, the test is carried out in an open-air 2km wireless environment. The time difference measurement results output by the Master device are used. And in the early stage, SR620 was used on the ground to measure the time interval of the 1PPS signal output by the devices at both ends, and at the same time, the log information of the time difference output by the Master device was read.

The measurement results of SR620 and Master are compared and verified, and the measurement errors of the two are 0.1ns (RMS) and 0.58ns (pp). Therefore, as shown in Figure 7, the time difference measurement result output by the Master can be used as the time difference measurement result in a dynamic wireless scenario.

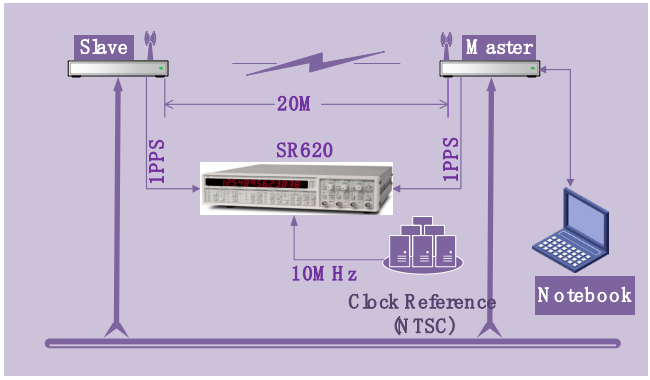

Figure 6. Experimental setup for 20m ground experiment

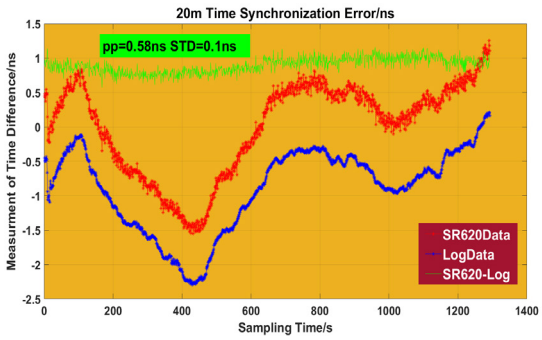

Figure 7. Ground static time synchronization test results (The distance between the master and the slave is 20m)

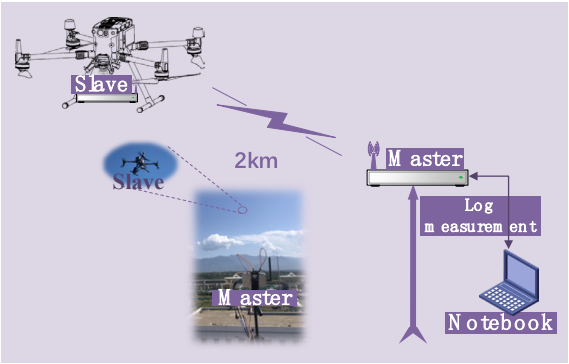

Figure 8. Experimental setup for 2km wireless flight experiment

The 2km wireless flight experiment principle and experiment site scene are shown in the Figure 8. The master station is placed on a bracket on the ground, the slave station is mounted on the DJI M300 UAV, and the notebook computer reads the time difference measurement data of the two stations from the master station in real time, and performs synchronization error analysis. The analysis results are shown in the Figure 9. The time synchronization accuracy

of the whole flight is 4.5ns (RMS). When the M300 starts to hover, the time difference begins to converge, and the time synchronization accuracy is 0.8ns (RMS) and 1.5ns (PP) after convergence.

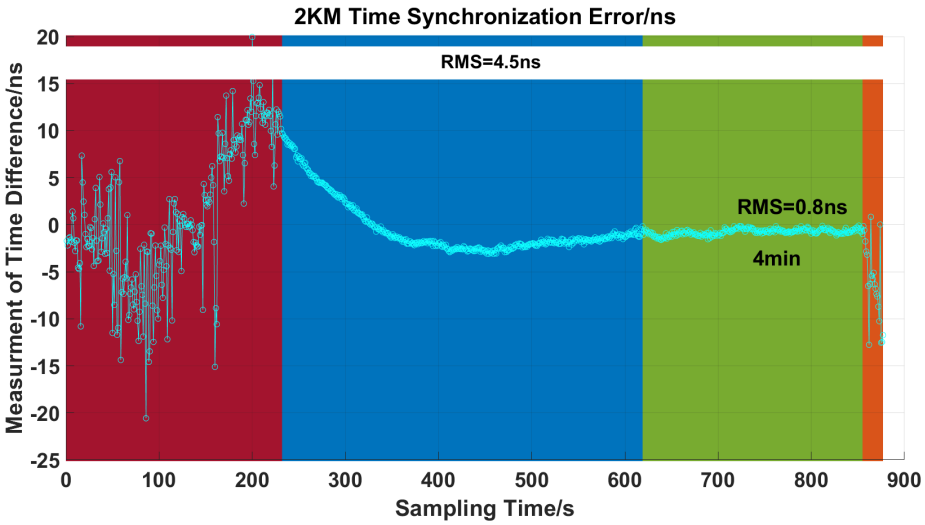

Figure 9. Time synchronization error of 2km flight experiment
(Red: fly away. Blue: hover converging. Green: hover converged. Orange: fly back)

3.2 Frequency Synchronization

To test the frequency synchronization performance between the Master device and the Slave device, a frequency synchronization performance test scenario is built, as shown in Figure 10. The master device and the measuring instrument are respectively connected to the 10MHz external reference from NTSC (National Time Service Center, CAS), and the slave end performs frequency synchronization with the master end through a microwave bidirectional link. Then test the 100MHz frequency performance of Master and Slave respectively by Microchip 53100A and Keysight 53230A. Frequency accuracy measurements can be read directly from the 53100A. The frequency accuracy needs to be processed as follows according to the frequency count result of the 53230A.

$$acc = \frac{1}{n}\sum_{k=1}^{n}\frac{\left|freq_k - 100e6\right|}{100e6}, \tag{13}$$

where $freq_k$ is the *kth* frequency measurement.

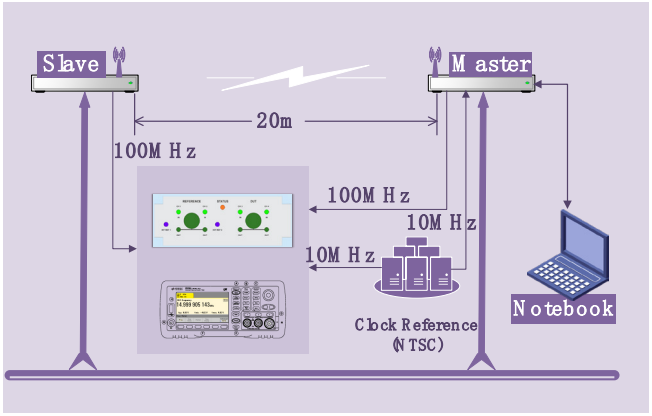

Figure 10 Experimental setup for frequency synchronization performance

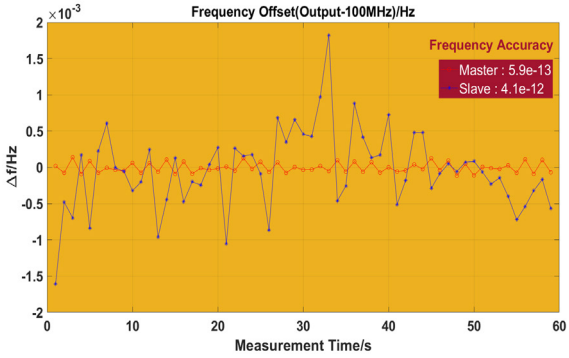

Figure 11. Measurement results of frequency accuracy

As shown in the Figure 11 and Figure 12, the frequency transfer stability of 100MHz is better than 3.8e-11(@1S), and the frequency accuracy is better than 4.1e-12.

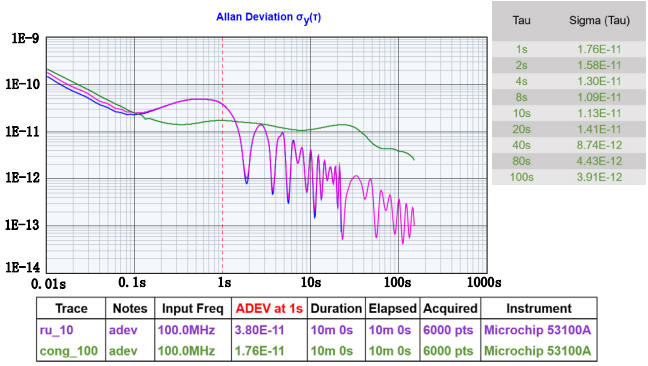

Figure 12. Frequency stability test results
(Green: master. Purple: slave)

4 Conclusion

In this paper, we presented our proposed TWTFRTS device in an FPGA-based hardware design, which was aimed for use in netted radar or coherent accumulation processing in multistatic radar imaging [13]. The time synchronization for the radar nodes could be achieved by using the proposed TWTFRTS device. The design, which takes advantage of the Two Way Satellite Time Frequency Transfer (TWSTFT) and GPS Decline Oscillator (GPSDO) and an adaptive algorithm for jitter elimination based on Kalman and PID, provided high accuracy for time synchronization performance. Experimental results with outdoor fight test of drone mounted with our device verified the accuracy of the proposed algorithm and hardware implementation of the TWTFRTS device. As shown in Table 1, the fight test showed that it had only a 0.8ns (RMS) and a 1.5ns (PP) time synchronization performance after the drone with our equipment hovered at 2km. The frequency stability of slave achieved 3.8e-11(ADEV@1S) and master achieved 1.8e-11(ADEV@1S), and the frequency accuracy of slave achieved 4.1e-12 and master achieved 5.9e-13 with the outdoor experiment, proving the advantages of the proposed hardware implementation and software design. The author in [14] proposed a time synchronization scheme and gave the test results in practical engineering applications (5ns peak-to-peak), but did not introduce the test conditions and test platform in detail. The authors in [8] presented autonomous GPS-disciplined oscillator in an FPGA-based hardware design, which was aimed for use in wireless sensor network nodes. Although [8] provided comparable frequency stability performance, its time synchronization performance is limited. The comparison of the proposed TWTRTS and the previous works is shown in Table 2.

Table 1 Measurement of time-frequency synchronization

Δ1*PPS*	Distance	100MHz Stability	100MHz Accuracy	Weight
0.8ns (rms) 1.5ns (p-p)	＞ 2km	3.8e-11 (slaver) 1.8e-11 (master)	4.1e-12 (slaver) 5.9e-13 (master)	800g

Table 2. Comparison of the proposed TWTRTS and the previous works

	Δ1*PPS*	Frequency stability
[14]	5ns (p-p)	--
[8]	0.356 μs (mean)	4.0e-11
This work	1.5ns (p-p)	3.8e-11

In the next step, we will partially inherit of satellite-ground time synchronization technology [15-19] and analyse the errors from seven aspects, including spatial distance error, transmission and reception channel delay error, receiving measurement error, multipath effect error, frequency synthesis error, antenna phase centre error, and clock error correction model error, aiming to further Improve the time synchronization performance of the system. In addition, more optimized estimation models for synchronization results may be further extended to quantum optimization algorithm [20]. In the longer term, we may also consider it from the perspective of optical disseminations [21].

Acknowledgments

This research was supported by National Natural Science Foundation of China (Grant No. 11973045), “Western Young Scholars” Program of the Chinese Academy of Sciences (Grant No. XAB2021YN23).

References

[1] J. Shen, A. Wang, C. Wang, N. N. Xiong, A RFID Based Localization Algorithm Applying Trilateration for Wireless Sensor Networks, *Journal of Internet Technology*, Vol. 18, No. 5, pp. 1167-1175, September, 2017.

[2] Y. Ge, P. Dai, W. Qin, X. Yang, F. Zhou, S. Wang, X. Zhao, Performance of Multi-GNSS Precise Point Positioning Time and Frequency Transfer with Clock Modelling, *Remote Sensing*, Vol. 11, No. 3, Article No. 347, February, 2019.

[3] L. Xu, X. Li, Y. Xue, A New Timing Method Based on Common-view, *IEEE Frequency Control Symposium*, Baltimore, MD, USA, 2012, pp. 1-4.

[4] F. Basile, T. Moore, C. Hill, G. Mcgraw, A. Johnson, Two Are Better Than One: Multi-Frequency Precise Point Positioning Using GPS and Galileo, *GPS World*, Vol. 29, No. 10, pp. 27-37, October, 2018.

[5] D. Kirchner, Two-Way Satellite Time and Frequency Transfer (TWSTFT): Principle, Implementation, and Current Performance, in: W. Stone (Eds.), *Review of Radio Sciences 1996–1999*, Oxford: Oxford University Press, 1999, pp. 27-44.

[6] V. Zhang, T. E. Parker, J. Achkar, A. Bauch, L. Lorini, D. Matsakis, D. Piester, D. Rovera, Two-Way Satellite Time and Frequency Transfer Using 1M Chip/S Codes, *Proceedings of the 41st Annual Precise Time and Time Interval (PTTI) Systems and Applications Meeting*, Santa Ana Pueblo, New Mexico, USA, 2009, pp. 371-382.

[7] S. Zhang, W. Yang, X. Wang, H. Wang, J. Ge, Review of Recent Progress of Two-way satellite time and frequency transfer, *Navigation Positioning and Timing*, Vol. 8, No. 4, pp. 11-19, April, 2021.

[8] T. Q. T. Bui, A. Elango, R. J. Landry, FPGA-Based Autonomous GPS-Disciplined Oscillators for Wireless Sensor Network Nodes, *Sensors (Basel)*, Vol. 22, No.9, Article No. 3135, May, 2022.

[9] J. S. Sandenbergh, M. R. Inggs, A Common View GPSDO to Synchronize Netted Radar, *IET International Conference on Radar Systems*, Edinburgh, UK, 2007, pp. 1-5.

[10] J. S. Sandenbergh, M. R. Inggs, Synchronizing Network Radar Using All-in-view GPS-disciplined Oscillators, *IEEE Radar Conference*, Seattle, WA, USA, 2017, pp. 1640-1645.

[11] Y. Diao, M. Li, X. Zhang, X. Wang, Satellite

Disciplined Crystal Oscillator System Based on Kalman Filter and PI Algorithm, *IEEE Conference on Industrial Electronics and Applications*, Hangzhou, China, 2014, pp. 624-628.

[12] H. Li, X. Zhang, Z. Li, H. Pan, W. Mao, Y. Yan, B. Yu, J. Tang, A Novel High-Precision Method Based on Sequence Weighted Adaptive Unscented Kalman Filter for GPS Disciplined Crystal Oscillator, *IEEE PES Asia-Pacific Power and Energy Engineering Conference*, Nanjing, China, 2020, pp. 1-5.

[13] G. Krieger, M. Younis, Impact of Oscillator Noise in Bistatic and Multistatic SAR, *IEEE Geoscience & Remote Sensing Letters*, Vol. 3, No. 3, pp. 424-428, July, 2006.

[14] B. Shu, Theory and Application of Two-Way Time Transfer Synchronization Technology, *Telecommunication Engineering*, Vol. 49, No. 1, pp. 63-66, January, 2009.

[15] X. Zhang, System Design and Key Technologies of High Accuracy Time and Frequency Microwave Link for Space Station, *Telecommunication Engineering*, Vol. 57, No. 4, pp. 407-411, April, 2017.

[16] Y. Guo, Y. Bai, S. Gao, Z. Pan, Z. Han, Y. Gao, X. Lu, A Satellite-Ground Precise Time Synchronization Method and Analysis on Time Delay Error Caused by Motion, *China Satellite Navigation Conference Proceedings*, Nanchang, China, 2021, pp 158-171.

[17] P. Delva, F. Meynadier, C. Le Poncin-Lafitte, P. Laurent, P. Wolf, Time and Frequency Transfer with A Microwave Link in the ACES/PHARAO Mission, *European Frequency & Time Forum*, Gothenburg, Sweden, 2012, pp. 28-35.

[18] A. Seidel, M. P. Hess, J. Kehrer, W. Schafer, M. Kufner, M. Siccardi, L. Cacciapuoti, I. A. Sanches, S. Feltham, The ACES Microwave Link: Instrument Design and Test Results, *IEEE International Frequency Control Symposium*, Geneva, Switzerland, 2007, pp. 1295-1298.

[19] H. Liang, S. Wang, Yu. Bai, S. Sun, L. Wang, Real-time frequency transfer system over ground-to-satellite link based on carrier-phase compensation at 10^{-16} level, *Chinese Physics B*, Vol. 30, No. 8, Article No. 080601, July, 2021.

[20] P. Singh, FQTSFM: A Fuzzy-Quantum Time Series Forecasting Model, *Information Sciences*, Vol. 566, pp. 57-79, August, 2021.

[21] Q. Shen, J. Guan, J. Ren, T. Zeng, L. Hou, M. Li, Y. Cao, J. Han, M. Lian, Y. Chen, X. Peng, S. Wang, D. Zhu, X. Shi, Z. Wang, Y. Li, W. Liu, G. Pan, Y. Wang, Z. Li, J. Wu, Y. Zhang, F. Chen, C. Lu, S. Liao, J. Yin, J. Jia, C. Peng, H. Jiang, Q. Zhang, J. Pan, Free-space dissemination of time and frequency with 10^{-19} instability over 113 km, *Nature*, Vol. 610, No. 7933, pp. 661-666, October, 2022.

Biographies

Ke Zhang is currently an assistant researcher of National Time Service Center, Chinese Academy of Sciences. He started his Ph.D. studying in 2021 at University of Chinese Academy of Sciences. He received MS in University of Chinese Academy of Sciences in 2017, and BS in Xidian University, China. His interest fields are Satellite navigation receiving technology, time frequency synchronization, baseband signal processing.

Decai Zou is currently a professor and Ph.D. tutor of National Time Service Center, Chinese Academy of Sciences. His research interests are satellite navigation, multi-source fusion navigation and positioning.

Pei Wang is currently a senior engineer at National Time Service Center, Chinese Academy of Sciences. He received Ph.D. in University of Chinese Academy of Sciences in 2017. His research interests are pseudo-satellites technology, time-frequency circuit design.

Wenfang Jing is currently a professor and Ph.D. tutor of National Time Service Center, Chinese Academy of Sciences. Her research interests are in the fields of microwave time and frequency transfer, navigation and communication.